PACS numbers: 61.72.up, 62.20.Qp, 68.35.bd

INFLUENCE OF HIGH-DOSE ION IMPLANTATION OF NiTi EQUIATOMIC ON SHAPE MEMORY AND PSEUDOELASTIC

Alexander Pogrebnjak[1], Sergey Bratushka[1], Neonila Levintant-Zayonts[2], Leonid Malikov[3]

[1]Sumy State University
Ukraine
[2]Institute of Fundamental Technological Research, PAS (Warsaw)
Poland
[3]Scientific Center of Physical Technologies of MES YS and NAS Ukraine (Kharkiv)
Ukraine

Received 13.08.2012

This work explains the method alloying process of the TiNi thin films in addition to the shape memory properties of the TiNi thin films made by alloying the TiNi multilayer thin films. The surface layer of an equiatomic TiNi alloy, which exhibits the shape memory effect in the martensitic slate, is modified with high-dose implantation ions N^+, Ni^+-N^+, and Mo^+-W^+ ions at a dose of $10^{17} – 10^{18}$ cm^{-2} and studied by Rutherford back scattering, scanning electron microscopy, energy dispersive spectroscopy, X-ray diffraction, and by measuring the nanohardness and the elastic modulus. After double implantation ions, the hardness of the TiNi samples is 2.78 ± 0.95 GPa at a depth of 150 nm and 4.95 2.25 GPa at a depth of 50 nm; the elastic modulus is 59 GPa. The coating demonstratedthe increased corrosion resistance in acidic and alkaline media in comparison with that of the non-implanted surface. A correlation between the elemental composition, microstructure, shape memory effect, and mechanical properties of the near-surface layer in TiNi is found.

Keywords: shape memory; pseudoelastic; implantation, NiTi, properties.

В работе предложен метод модификации свойств тонких пленок TiNi с эффектом памяти формы путем легирования и формирования многослойных пленок. Поверхностный слой эквиатомного сплава TiNi, обладающего эффектом памяти формы в мартенситной фазе, изменялся путем высокодозной имплантации ионов N^+, Ni^+-N^+ и Mo^+-W^+ с дозой $10^{17}– 10^{18}$ $см^{-2}$ и исследовался методами Резерфордовского обратного рассеяния, сканирующей электронной микроскопии, энергодисперсионной спектроскопия, дифракции рентгеновских лучей. Дополнительно измерялись нанотвердость и модуль упругости. Обнаружено, что при двойной имплантации ионов микротвердость образцов TiNi составляет 2.78 ± 0.95 ГПа на глубине 150 нм и 4.95 ± 2.25 ГПа на глубине 50 нм, а модуль упругости 59 ГПа. По сравнению с неимплантированной поверхностью покрытие обладает повышенной коррозионной стойкостью в кислых и щелочных средах. Обнаружена корреляция между элементным составом, микроструктурой и эффектом памяти формы и механическими свойствами приповерхностного слоя TiNi.

Ключевые слова: эффект памяти формы, псевдоупругость; имплантация, NiTi, свойства.

У роботі запропоновано метод модифікації властивостей тонких плівок TiNi з ефектом пам'яті форми шляхом легування та формування багатошарових плівок. Поверхневий шар еквіатомного сплаву TiNi, що має ефект пам'яті форми в мартенситній фазі, змінювався шляхом високодозної імплантації іонів N^+, Ni^+-N^+ та Mo^+-W^+ з дозою $10^{17} – 10^{18}$ $см^{-2}$ і досліджувався методами Резерфордівського оберненого розсіювання, скануючої електронної мікроскопії, енергодисперсійної спектроскопії, дифракції рентгенівських променів. Додатково вимірювалися нанотвердость і модуль пружності. Виявлено, що при подвійний імплантації іонів мікротвердість зразків TiNi становить 2.78 ± 0.95 ГПа на глибині 150 нм та 4.95 ± 2.25 ГПа на глибині 50 нм, а модуль пружності становить 59 ГПа. У порівнянні з неімплантірованною поверхнею покриття має підвищену корозійну стійкість у кислих і лужних середовищах. Виявлено кореляцію між елементним складом, мікроструктурою та ефектом пам'яті форми і механічними властивостями приповерхневого шару TiNi.

Ключові слова: ефект пам'яті форми, псевдопружність; імплантація, NiTi, властивості.

 © Alexander Pogrebnjak, Sergey Bratushka, Neonila Levintant-Zayonts, Leonid Malikov, 2012

INTRODUCTION

Shape memory alloys (SMAs) possess an array of desirable properties: high power to weight ratio, thus the ability to recover large transformation stress and strain upon heating and cooling, pseudoelasticity (PE), high damping capacity, good chemical resistance and biocompatibility. This attracted much attention to the research of SMAs as smart and functional materials [1]. Among these SMA films, TiNi based films are the most promising ones.

Research related to application of TiNi alloys in medicine started in the late sixties. TiNi alloys became attractive for medical applications particularly because of memory properties. Ability of TiNi elements to recover an original shape after being deformed up to almost 10% offers a considerable improvement during numerous medical treatments. For instance a tailored compressive fixation of bone fragments (e.g. fragments of small bones, broken jaws, cranial fractures) can be easily performed using recoverable deformation. Anchoring of implants (e.g. tooth roots, joint implants) and dentures to the living tissues as well as positioning of tissues (e.g. shifting of misaligned teeth or vertebra, opening of narrowed veins or urethral tracts) is easily achievable using TiNi articles exhibiting shape memory behavior. Forces generated by memory elements can be controlled and invasive interventions can be minimized. Actuating ability of shape memory articles allows replacement or support of damaged muscles and tendons. Unique memory properties allow designing unique medical instruments with excellent steerability and flexibility (e.g., endoscopes). In addition to memory properties, TiNi shape memory alloys exhibit significantly better mechanical compatibility with tissues compared to other alloys and ceramics used in medicine. TiNi alloys exhibit excellent corrosion resistance, wear resistance, mechanical damping capacity, MRI visibility and sufficient radio-opacity [2].

The phase transformation in SMA thin film is accompanied by significant changes in the mechanical, physical, chemical, electrical and optical properties, such as yield stress, elastic modulus, hardness, damping, shape recovery, electrical resistivity, thermal conductivity, thermal expansion coefficient, surface roughness, vapor permeability and dielectric constant, etc. These changes can be fully made use of the design and fabrication of microsensors and microactuators. The fatigue life and sharpness of the TiNi tool is excellent compared to steel because of SIM formation and greater wear resistance and corrosion stability. The PE and SME were also utilized in instruments with a non-traumatic tissue retractor, repositioning devices [3] or markers. Chisels, scissor forceps, saws and blades made of TiNi alloys, which do not use SME or PE are effective due to their excellent wear and corrosion resistance. However, due to the lack of full understanding of the thin film SMAs together with the difficulty in controlling of the deposition parameters, they have not received as much attention in the technology as other microactuator technologies [2].

The introduction of a third component (for example – Si or B) into the films may markedly improve their physico-mechanical properties and thus extend the scope of application. Chromium is known to have a beneficial effect on the stability of titanium carbides, borides and nitrides against oxidation and on the wear resistance of articles made of them at elevated temperatures.

The application of high-dose intense implantation leads to an increase in the ion penetra-tion depth; intensified scattering of the surface layer; a shift in the maximum, concentration, and shape of the concentration profile; and many other processes that are weakly pronounced during low-intensity ion implantation at low doses (several units of atomic processes) of implanted ions [4 – 6]. On the other hand, TiNi-based alloys belong to the group of materials in which a high-temperature phase with a B_2 structure undergoes a shear or martensitic phase transformation as the tem-perature changes or a stress is applied. The atomic restructuring in TiNi-based alloys is accompanied by both martensitic anelasticity effects and a change in their surface state, which is caused by the complex structure of the martensite phase in them [7, 8].

As a result, a developed martensitic relief with a large num-ber of various interfaces appears, which should affect both the electrochemical and corrosion properties and the plasticity and strength properties of these materials. As a method of surface alloying, ion implantation of a surface can strongly affect the structural parameters and stability of the B_2phase in the near-surface layers and, hence, the following set of its properties: the martensite transformation temperature, the martensiteanelasticity parameters, the shape memory effect (SME), and superplaslicity. As a result, it can change the deformation relief, the

cracking conditions, and the electro-chemical and corrosion properties [9 – 14]. Therefore, double implantation of N^+ and Ni^+ ions into TiNi is of particular interest, since the implantation of Ni^+ ions changes the equiatomic composition of the alloy and. in combination with N^+ ions, hardens the surface layer and. correspondingly, modifies the physico-mechanical and chemical properties [15]. The effect of N^+ ions on the mechanical properties of steels and alloys is well known. The alloying of steels and alloys with elements such as W and Mo is widely used to improve their mechanical properties; therefore, it is interesting to perform implantation of Mo^+ and W^+ ions at high doses. The purpose of this work is to study the depth profile of the elemental com-position of the implanted layer, the structure and morphology of the TiNi alloy surface, and the mechanical properties of the alloy implanted by high doses of N^+, $Ni^+ + N^+$ and $W^+ + Mo^+$ ions at doses ranging from $5 \cdot 10^{17}$ to 10^{18} cm^{-2} [16, 17].

METHODS OF ANALYSIS AND COATING APPLICATION

We analyzedequiatomicTiNi (51.5% Ni) alloy samples 22×5.4×0.25 mm in size. In the initial state, the samples were vacuum annealed at 803 K for 30 min followed by slow cooling. After cooling, the sample surfaces were etched with a mixture of 10% $HClO_4$ and 90% acetic acid. The N^+ ion implantation of the TiNi samples was performed on a semi-industrial IMJON (Warsaw) implanter at doses of $1 \cdot 10^{17}$, $5 \cdot 10^{17}$, and 10^{18} cm^{-2} at a current density of 0.8 – 1 mA. The implan-tation of Ni^+ and $Mo^+ + W^+$ ions was carried out using a vacuum-arc Diana source at a voltage of about 60 kV, a dose of $5 \cdot 10^{17}$ cm^{-2}, and a substrate temperature of less than 250 °C. Irradiation was performed at a pres-sure of ~10^{-3} Pa. The pulse duration was 200 мs, the pulse repetition frequency was 50 Hz, and the nitrogen concentration in TiNi was determined from the "eating away" in its energy spectrum. The phase-transformation temperatures were determined with a Pyris-1 differential scanning calorimeter, and the elemental composition of the samples was determined by the following methods: Auger electron spectroscopy on a PHI-660 (Perkin-Elmer) device, scanning electron microscopy on a Selmi (Sumy. Ukraine) microscope equipped with EDS and WDS microanalyses and on a Perkin-Elmer microscope, and Rutherford backscattering of ions (2.012 MeV proton beams. 2.035 MeV $^+$He ion beams). Rutherford backscattering spectra were analyzed using the standard RUMP and DWBS software packages [18] to construct the depth profiles of elements (Ni^+, Mo^+, W^+ ions). Ions backscattered at an angle of 170° were detected using a surface barrier detector with an energy resolution of 20 keV. In addition, we used a Neophot-2 optical micro-scope. To measure the mechanical properties and SME, we used a diamond pyramid (Brinel) microindenter) with a side of 40 nm at a load of 4, 7, 10, 13, 16 and 20 N and a Talysurt-5-120 scanning profilometer. The measurements were performed in the initial state and after ion implantation.

The microhardness on the surface of a sample and across it was measured with a PMT-3 device at various loads. The nanohardness was measured with a trihedral Berkovich pyramid on a Nano Indenter II (MTS System Corp., Ridge. Tennessee, United States) nanohardness tester. To find the hardness and the elastic modulus at the maximum load, we used the Oliver-Pharr technique [19].

X-ray diffractometry, using the Philips diffractometer type X'Pert in the Bragg-Brentano geometry, was used to identify the phase composition of NiTi alloy samples in both non-implanted conditions and after implantation with nitrogen. CuK_α radiation (wavelength λ – 0.154184 nm) diffracted by the sample was selected by a graphite monochromator. The scanning voltage of the X-ray tube was 40 kV, the current was 25 mA, the exposure time was 10 s and the measured angle, 2Θ, was from 25° to 95°. The scanning step was 0.02°. The low temperature X-ray diffraction studies were carried out using the TTK Low-Temperature Camera (Anton Paar). The sample was heated from –50 °C up to +150 °C in argon atmosphere. The measured angle, 2Θ, was from 35° to 47° with the scanning step of 0.02°. Lattice parameters were deter-mined by using the Philips X'Pert Plus software for all detected peaks.

Specimens for TEM and HREM (Tecnai G^2. FEI Company) examinations were prepared by Focused Ion Beam System (FEI QUANTA 3D).

RESULTS AND DISCUSSION

The studies were started with DSC measure-ments. The sample weight of approximately 5 mg was analyzed with an empty aluminum pan as the reference. A temperature range from –50 °C to +150 °C was

scanned at a rate of 20 °C/min during cooling and heating. Fig. 1 shows the evolution of DSC cooling/heating curves for the virgin and ion-implanted alloys. As it can be seen, the NiTi alloy transforms in two steps showing two peaks on the DSC curve in the cooling direction. The first DSC peak correlates with the transformation from the austenite (A)with a cubic structure (B_2-phase) to the R-phase with a rhombohedral one (referred to as a rhombohedral distortion of the austenite). The second DSC peak correlates with the transformation from the R-phase to the martensite (*M*) with a monoclinic structure ($B_{19'}$-phase).

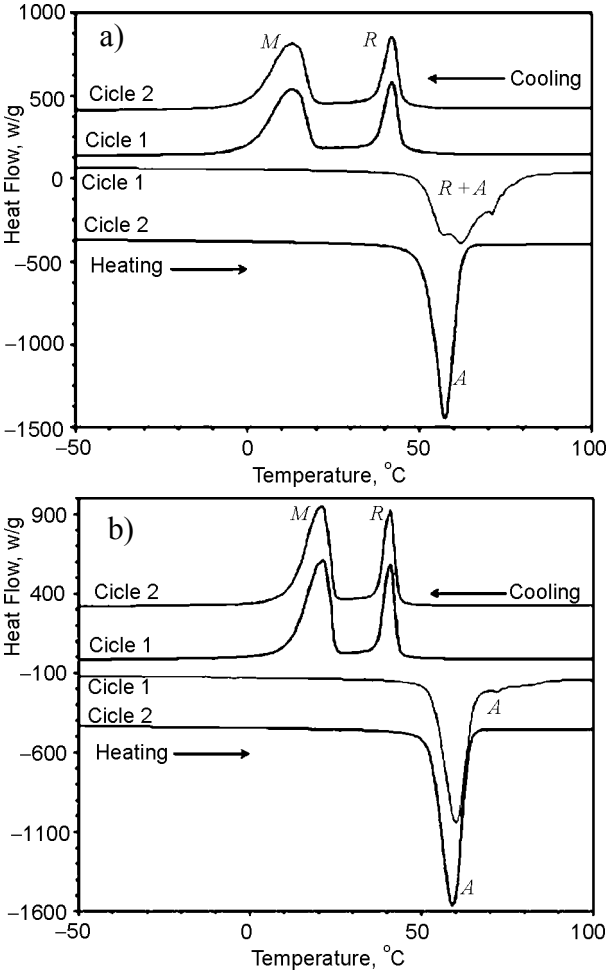

Fig. 1. (a) DSC curves of the virgin NiTi alloy. (b) DSC curves of ion-implanted alloys indicating a two-step phase transformation occurred during cooling.

Similar two-step martensite phase transition from high temperature was observed for the NiTi alloys after the thermo-mechanical treatment or solution treatment and subsequent aging. The one-step but composed transition took place during the heating process. The endothermic peak during the heating process resulted in the transition of the martensite to the austenite phase. The peak in the heating direction corresponds to the austenite (B_2-phase) with t_{start} = 51.6 °C, t_{finish} = 62.3 °C for the virgin alloy and with t_{start} = 52.5 °C, t_{finish} = 64 °C for the ion-implanted one. The subscript 'start' denotes the onset temperature at which the phase transformation starts, and the 'finish' the temperature at which the phase transformation finishes.

Transformation temperatures M_f, M_s, A_s, A_f, T_R as well as their changes with applied stress must be determined experimentally. Temperature dependence of yield stress has to measured and temperature is estimated from cross-section of M_s and $R_{P0.2}$ dependencies. Proper design requires knowledge of the deformation behavior of particular TiNi SMA element at application temperatures. [2] Dependencies shown in fig. 2 must be determined for the deformation mode which will be applied in practice (e.g. compression, bending, torque etc.).

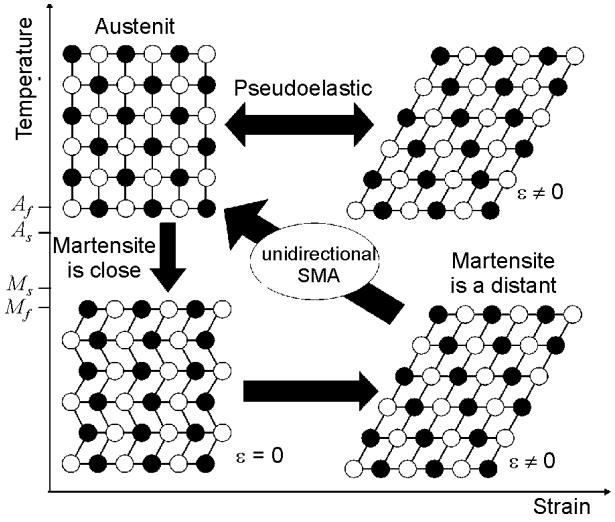

Fig. 2. Schematic representation of the mechanisms and effects SMA and PE.

The two peaks in the cooling direction corresponding to the R-phase and the martensite $B_{19'}$-phase were determined to have transformation temperatures, respectively: t_{start} = 45.1 °C, t_{finish} = 37.8°C, t_{start} = 19 °C, t_{finish} = 1 °C for the virgin alloy and t_{start} = 43.3 °C, t_{finish} = 37.4 °C, t_{start} = 24.6 °C, t_{finish} = 11.6 °C for an ion-implanted alloy. With Auger electron spec-troscopy, we also studied the TiNi samples before and after implantation with nitrogen ions. In the initial state, carbon and oxygen are present near the surface; after sputtering for 15 – 18 min. only nickel and titanium are present in the NiTi sample and their concentrations are close to the equiatomic composition. After implantation, the nickel concentration in the surface layer decreases to almost 10 at.%

because of sputtering of the surface. Since it is difficult to separate the peaks of nitrogen and titanium ions, we constructed a TiN profile with Auger electron spectroscopy.

This profile indicates that the penetration depth of N^+ ions is about 280 – 200 nm. After sputtering for 10 min the concentrations of nickel and titanium ions are seen to level off and reach their intrinsic levels (49.9 and 50.1 at.% Ni and Ti in the crystal lattice of the TiNi alloy, respectively).

Fig. 3 shows optical microscopy data. They demonstrate a typical martensitic structure and changes in the martensitic structure after implantation.

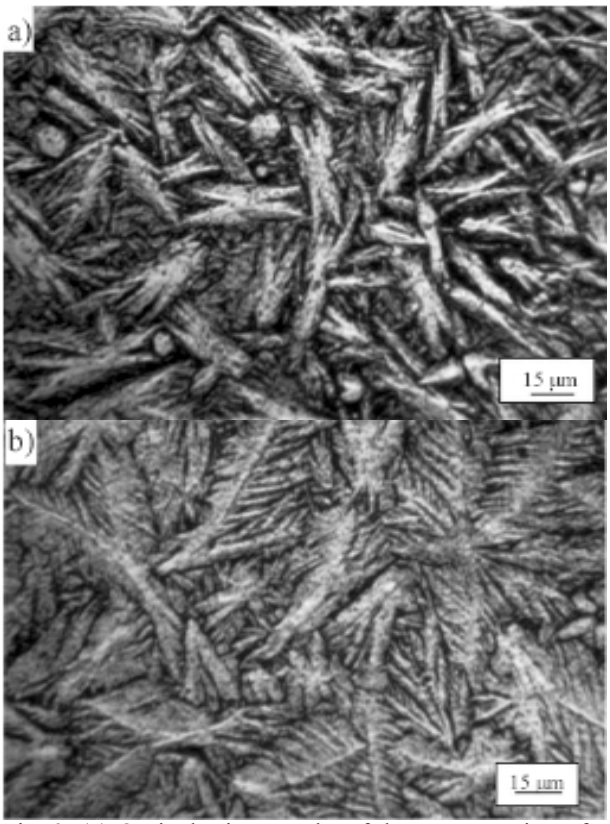

Fig. 3. (a) Optical micrographs of the cross-section of a TiNi alloy with a martensitic structure and SME before implantation. (b) Optical micrographs after ion implantation.

The surface layer of the implanted sample has a significant concentration of nitrogen and oxygen and the characteristic eating away is observed in the spectrum of TiNi implanted sequentially by nitrogen and nickel. We used a standard computer program and determined the nitrogen con-centration from the eating away in the spectrum and plotted element-concentration profiles. The eating away appears when a light element is added to a heavy-element matrix. The yield in a layer containing a light element decreases in proportion to a decrease in the heavy-element concentration. If the light-element concentration increases to 100%, a pure light-element layer forms. Therefore, we can easily determine the error in determining the concentration of nitrogen ions; it was found to be 5 at.%. The error in determining the nickel concentration for concentration profiles was 1.2 at.%. The nickel profile was plotted beginning from 50 at.%. This point was taken as an initial point, since the titanium or nickel concentration in the initial state is about 50 at.%.

When analyzing the profile of N^+ ions in TiNi (fig. 4), we see that the nitrogen profile has a double-humped shape: one concentration maximum is located near the surface (the maximum concentration is about 36 at.%). and the second peak is located at a depth of more than 130 – 150 nm (133 at E^2 and has a lower con-centration (27 at.%). In the valley between the two nitrogen concentration maxima, the concentration of Ni^+ ions is maximal (about 20 at.%).

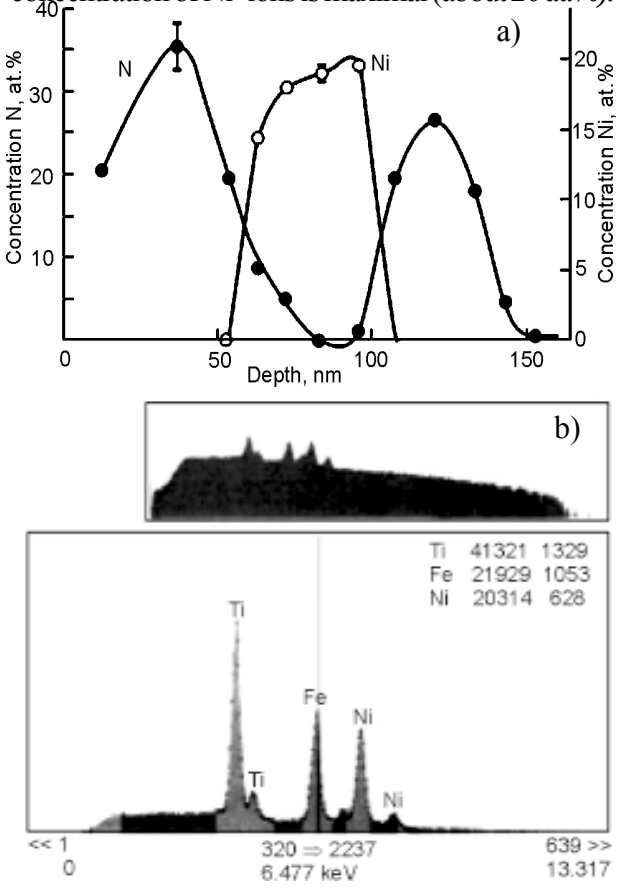

Fig. 4. (a) Depth profiles of the element concentrations obtained from energy spectra of the TiNi sample surface after double implantation of N ions at a dose of 10^{18} cm^{-2} and Ni ions at a dose of $5 \cdot 10^{17}$ cm^{-2}; (b) X-ray spectrum taken with WDS from the TiNi sample after double implantation by N and Ni ions.

Moreover, prelim-inary SIMS (secondary-ion mass spectrometry) studies also demonstrate the formation of a double-humped nitrogen concentration profile. However, the nitrogen concentrations

in the maxima differ slightly from the RBS data, which is caused by the higher threshold of delegability of SIMS (~10^{-5} at.%).

Three TiNi phases are important in shape memory phenomena. High temperature phase (austenite) has an ordered CsCl or B_2-type lattice. So-called "R-phase" with rhombohedral crystal lattice may form first upon cooling at T_R temperature. The second type of martensite has the monoclinic B_{19*} lattice. Transformation temperatures depend on chemical composition and structure of the TiNi alloy.

The R-phase is commensurate with B_2 lattice. An instability of B_2 structure and formation of so called incommensurate phase always precedes the formation of R-phase. The two sequences of phase transformations are possible in binary TiNi alloys [2, 20, 21]:

I $B_2 \rightarrow$ incommensurate phase $\rightarrow R \rightarrow B_{19'}$, or

II $B_2 \rightarrow B_{19*}$.

The R-phase formation precedes the B19' transformation when the Ms temperature is lowered (MS < TR). Increase of Ni content with respect to Ti, work hardening, and aging can depress the M_s and yield the R-phase formation [20 – 22]. The R-phase transition is typified by extremely narrow thermal hysteresis (1 to 2 °C). whereby thermal hysteresis related to B_{19*} may vary from approximately 20 °C to hundreds ot degrees [21]. By alloying the binary TiNi system with other elements, the effective control of transformation temperatures can be accomplished. Formation of orthorhombic martensite B_{19} instead of R-phase and $B_{19'} \rightarrow$ triclinic $B_{19''}$ martensite transformation have been detected in ternary systems.

Three factors influence the deformation behavior, corrosion behavior and shape memory parameters of TiNi alloys [2, 21, 22]:

1. chemical composition (content of Ti, Ni, alloying elements and impurities);

2. dislocation density and grain size of austenitic phase;

3. presence of coherent precipitate.

Any operation related to change of dislocation density and grain size, diffusion, and precipitation processes changes the transformation temperatures of TiNi. This is extremely important because the high temperature shape to be "memorized" by a TiNi alloy is most typically imparted at temperatures between 400 to 600 °C. Varying chemical composition and thermal and mechanical treatment of TiNi alloys represent an important tool in tailoring their performance. Recoverable strains during SME and PE in TiNipolycrystals vary up to 8% and generated stresses up to 1000 MPa have been reported. Increases in dislocation density after cold-work lead to decreases in recovery strain because of limitations (pinning) of interface movement. Work-hardened materials yield higher generated stresses compared to annealed TiNi alloys [2, 23, 24]. The M_s temperature decreases and the T_R and A_s temperatures increase after work hardening. Introduced structure defects result in widening of thermal hysteresis and widening of intervals between M_s and M_f or A_s and A_f respectively. The orientation dependence of properties, especially in the case of wrought TiNi specimens, is typically observed [2, 20, 23]. The structure parameters will also determine fatigue lifetimes.

The X-ray diffraction patterns of the ion-implanted NiTi alloy against the temperature are shown in fig. 5. From the results obtained it can be seen that alloys at 20 °C exhibit the three phases: the dominating $B_{19'}$-phase and a small amount of the R_2 and B_2 phases. The appearance of austenite phase (crystalline, nanocrystalline and/or amorphous-like) may be related to structural changes in the NiTi alloy during the ion implantation process and to high temperature of target. Appearance of the R-phase, similar to the results obtained for annealed materials, may be induced by high temperature of target. An increase of temperature in the material results in an increasing fraction of the B_2-phase. The diffraction patterns of this $B_{19'}$-phase do not vary up to 65 °C.

Above this temperature an increasing fraction of the B_2-phase and a distinctly decreasing fraction of the $B_{19'}$ one were observed. The $B_{19'} \rightarrow B_2$-phase transformation finishes above a temperature of 80 °C. The X-ray diffraction patterns obtained for the highest temper-atures (from 80 °C to 150 °C) contain only reflections from the B_2-phase.

Lowering the temperature up to about 41 °C, besides still existing B_2-phase, the R-phase appears. From the results obtained it can be seen that the $R \rightarrow B_{19'}$-phase transformation starts form a temperature of 25 °C and finishes about 25 °C. Along with the decreasing temperature, besides the dominating $B_{19'}$-phase, a small amount of the B_2-phase

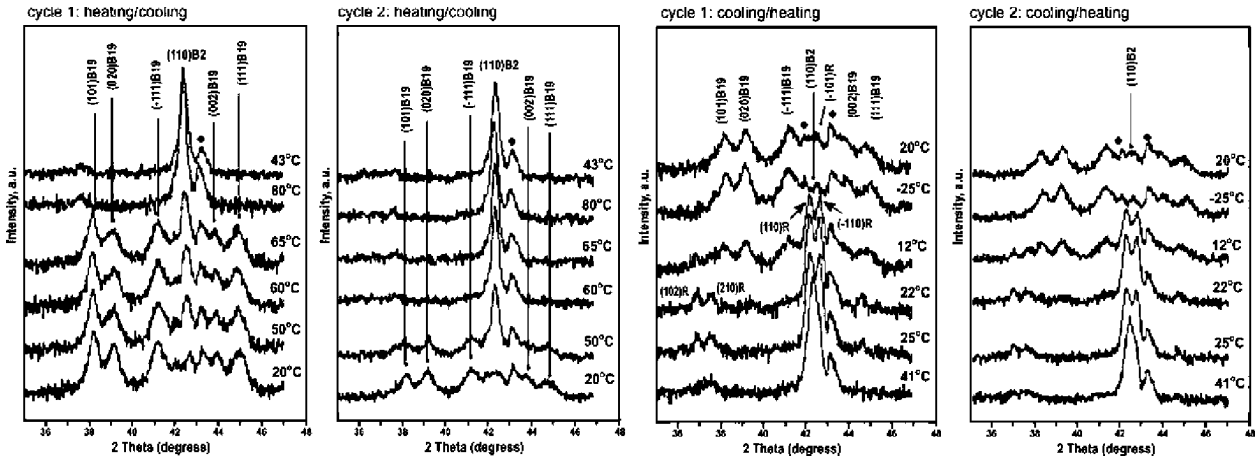

Fig. 5. Recorded X-ray diffraction patterns versus temperature of ion-implanted NiTi alloy at a fluence of 10^{18} cm^{-2} and energy 50 keV.

was detected. Such phase composition was also observed for the material at 20 °C on the start and finish of the second thermal cycle. The broad structure of this diffraction peak may testify that still some amount of the amorphised and/or nanocrystalline B_2-phase is present in the alloy. It should be noted that from the results obtained there is no evidence for TiN and Ti_2Ni compound formations.

In the process of nitrogen ion implantation with the fluency 10^{18} cm^{-2} and 50 keV of energy, the well-defined double-layer structure with different microstructure as well as different phase and chemical composition was formed (fig. 6). During ion implantation, collisions between the incident ions and the NiTi-target atoms lead to the formation of near-surface amorphized layer *(*A-layer, fig. 6a) and the extended defects in the crystalline structure of bulk material (D-layer, Bulk in fig. 6a).

The transition zone of a damaged region is wide and its composition changes gradually from totally amorphized Ti-rich material (heavily damaged and nano-crystalline) to Ni-rich crystalline (A1 and A2 regions in A-layer in fig. 6b, c). Amorphous-like layer contains some amount of crystalline inclusions within its bulk, mainly near a bottom boundary of the transition zone. This confirms the fact that the amorphization process occurs faster from the depth of maximum damage regions towards the sample surface than in its bulk. Due to differential strain between the undamaged and damaged layers, many cracks appear in this region. In the depth of 80 – 160 nm the material has a defected crystalline microstructure.

The TiNi samples implanted by N^+ ions are seen to have a higher (by 15 – 20%) hardness than the initial samples. The changes in the SME (fig. 7) demonstrate that the implanted TiNi alloy exhibits an indentation with a higher hardness after recovery as a result of healing to 75 °C. In other words, all mechanical changes related to the SME and mechanical properties (hardness) are interrelated with the elemental composition and micro-structure of the material. The hardness H and the elastic modulus E were determined using a nanohardness measuring device (Nanoindenter II) according to the Oliver-Pharr and Berkovich indentation methods. The

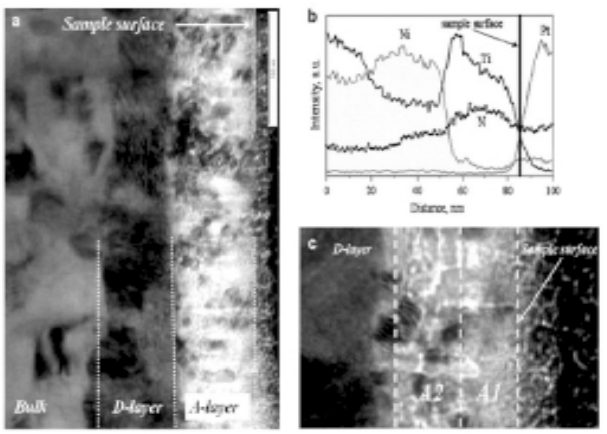

Fig. 6. (a) Bright-field image of the ion-implanted NiTi alloy demonstrating the structure. (b), (c) Chemical composition changes in near-surface layers.

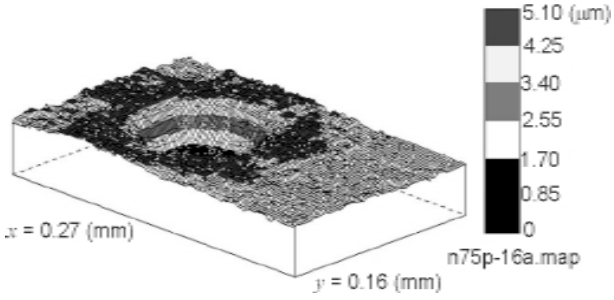

Fig. 7. SME measurements (with a scanning profilometer) on a TiNi sample after heating to 75°C.

hardness (H) and Young's modulus (E) data change correspondingly. Their values were determined at various depths (see tabl. 1).

Table 1

Hardness and elastic modulus of TiNi samples

Sample	E, GPa	H, GPa
depth of 150 nm		
Initial	56 ± 2	2.13 + 0.30
W + Mo	59 + 11	2.78 + 0.95
W + Mo after annealing	298 + 81	4.11 ± 0.35
depth of 50 nm		
Initial	56 ± 4	2.74 + 0.30
W + Mo	59 + 8	4.95 + 2.26
W + Mo after annealing	236 + 39	4.44 ± 1.45

The hardness is seen to increase from 2.13 ± 0.13 to 2.78 ± 0.95 GPa at a depth of 150 nm. The elastic modulus varies from E = 56 ± 2 to 59 ± 11 GPa. After annealing at 550 °C for 2 h, these values increase sharply: H = 4.11 ± 0.35 GPa, E = 289 ± 81 GPa (fig. 8). Small differences between the hardnesses and elastic module of the initial and implanted and annealed samples are also detected at a depth of 50 nm. Upon implantation, we have H = 4.96 ± 2.26 and E = 59 ± 8 GPa; after anneal-ing, we have H = 4.44 ± 1.45 and E = 236 ± 39 GPa (the elastic modulus increases by a factor of almost 4.5).

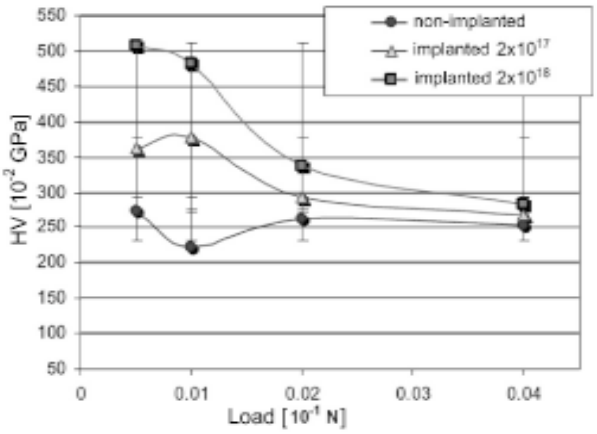

Fig. 8. Microhardness NiTi samples before and after implantation.

A value of elastic recovery W_e of a surface layer was calculated using the curves "loading-unloading". The penetration diagrams are shown in fig. 9a – c. A peculiarity of given diagrams is essentially high for a metal elastic recovery in indentor unloading. This indicates a low modulus of E elasticity with a relatively high hardness H (a value of the

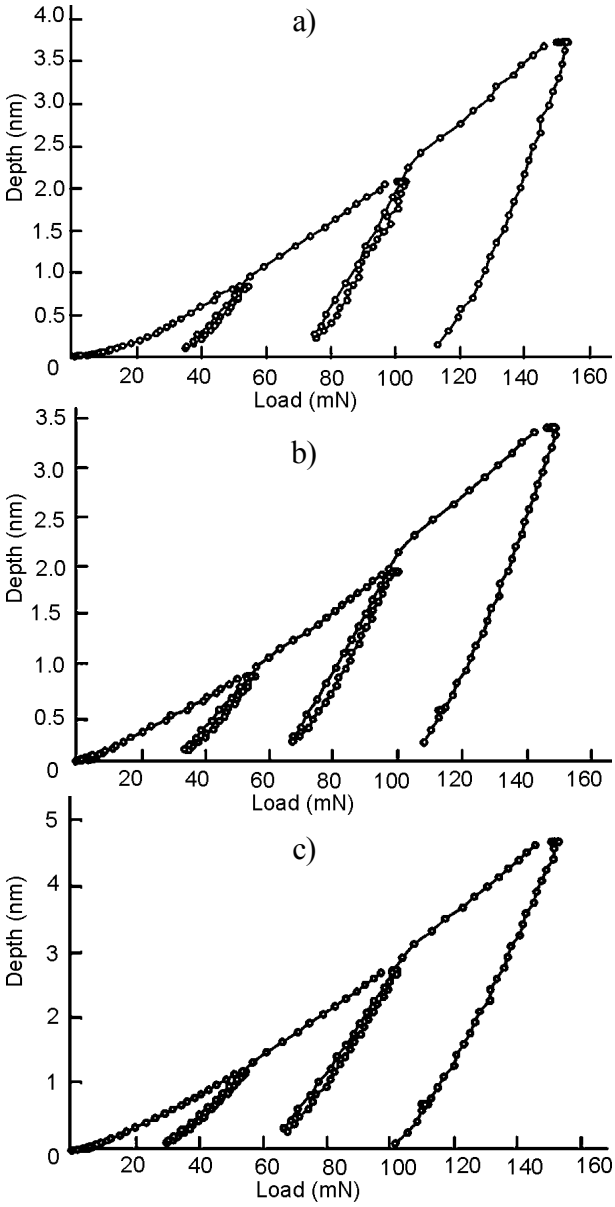

Fig. 9. (a) A diagram of indentation penetration for an initial sample. (b) A diagram after the implantation. (c) A diagram after the annealing.

elastic recovery was determined by the ratio E/H). A load which was necessary for indentor penetration to 50 nm depth was minimum for an initial sample (0.8 – 0.1 mH), increased to (0.9 0.1 mH) for an implanted sample and was maximum for an implanted sample after annealing (1.2 – 0.1 mH). This indicates growing hardness of the surface layer after implantation and annealing. The fact that an elastic recovery of a print depth in unloading after annealing was much longer than that for an initial one is worth our attention. This indicates that hardness growth was accompanied by weak modulus enhancement i.e. hardness after implantation and annealing increased more significantly than the elastic modulus.

Investigation of the influence of nitrogen ion implantation on the wear resistance of shape memory material was carried out on samples from equal tothe atomicalloy NiTi (Nitinol, Shape Memory Corporation, Japan) in the martensitic phase. Samples of size 22Ч5,4Ч0,3 mm annealed for 30 min in a vacuum oven at 583 K, and then washed in a solution of 10% $NClO_4$ 90% CH_3COOH. Nitrogen im-plantation was carried out at doses of $D_1 = 1 \cdot 10^{17}$ J/cm^2) and $D_2 = 2 \cdot 10^{18}$ J/cm^2) at a beam energy of 50 – 65 keV ions. The wear resistance of the surface layer at friction was carried out using a sapphire ball tribologicaltester 6 mm in diameter with a piston sliding without lubrication on the surface of the material.

In testing, the ball was loaded with a load of 0.4 N and 0.70 N, and the amplitude of the reciprocating motion of the ball was 3 mm. The wear resistance were investigated non-implanted and implanted (doses D_1 and D_2) samples of alloy NiTi. The test was 1:00, 3:00, 6:00 and 12:00 hours. To obtain reproducible results for each attempt (for different values of load and time) tests for all samples were repeated three to five times. After moving the ball on the surface of the load visible signs of wear (tracks) in the form of grooves. The depth of the furrows can judge the degree of wear of the material. Measure of ash material can serve as the volume of the furrow. Additionally, after the wear test were carried out in profilometrics measurements obtained by furrows, which allowed the comparison of surface morphology. Using the software, Hommel Map Expert maps were constructed surface under study, allowing to show signs of wear on the surface of NiTi upside down, allowing to observe that the "bottom" grooves, resulting in friction (fig. 10).

After ion implantation modified samples showed greater resistance to abrasion of the surface layer compared to non-implanted material. The dependence of the flow of material NiTi before and after

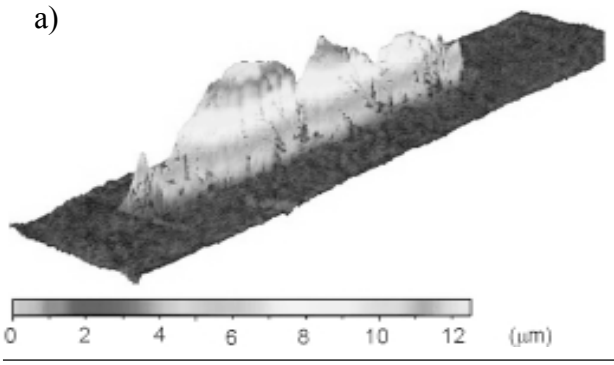

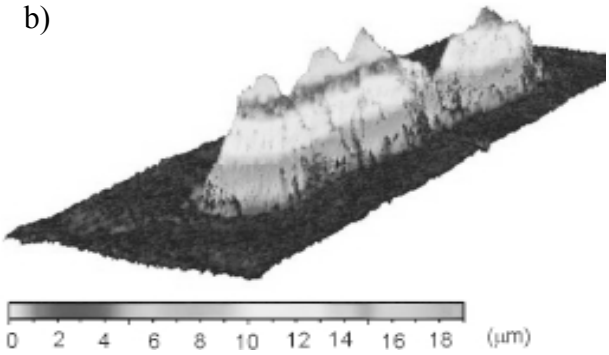

Fig. 10. (a) Examples of profiles of wear of the alloy NiTi: an inverted trace of wear surfaces non-implanted NiTi (load 0.4 N / friction during 12 h). (b) Profiles of wear of the implanted NiTi alloy (load 0.7 N / friction during 6 h)

ion implantation during "dry sliding" friction in the test of time (under a load of 0.7 N and 0.4 N) is shown in fig. 11. For both loads (0.4 N and 0.70 N) at any time in the abrasion test (1:00, 3:00, 6:00 and 12:00 hours) the amount of material blown from the implanted samples was lower than for non-implanted material.

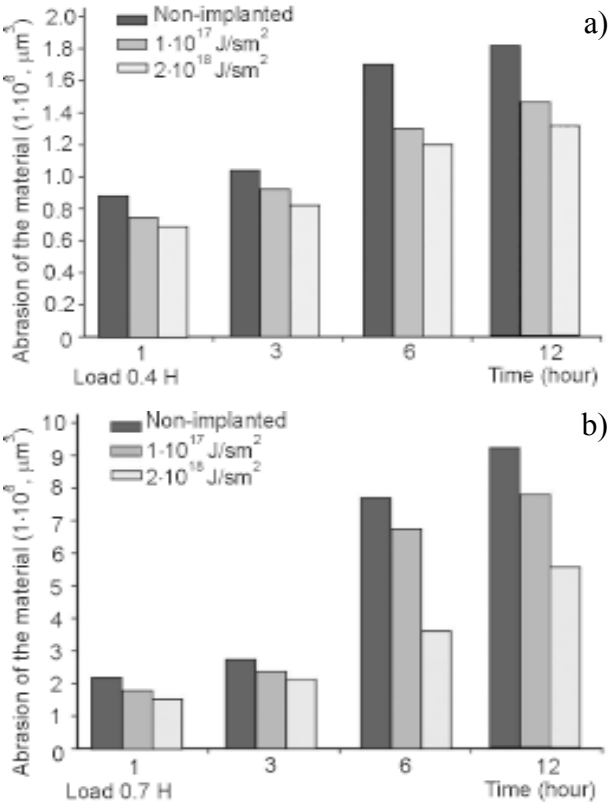

Fig. 11. (a) Consumption NiTi before and after ion implantation ($D_1 = 1 \cdot 10^{17}$ J/cm^2 and $D_2 = 2 \cdot 10^{18}$ J/cm^2) during "dry sliding" test of time: for the load 0.4 N. (b) Consumption NiTi for the load 0.7 N.

In the case of load 0.4 N (fig. 11a) at a dose of implantation D_2 increased wear resistance was higher not only compared to non-implantedsamples,

but also in comparison with the samples modified at a lower dose of D_1. After 1 h of friction ball difference between the ash material for all samples is negligible. Significant differences in the amount of material blown from the non-implantedand implanted samples visible during the test due to friction at 3 h, 6 h and 12 h. As can be seen from fig. 11b, at a load of 0.7 N increases the wear resistance of samples implanted with a dose of D_2 NiTi noticeable not only in relation to the non-implantedsamples, but also implanted with a lower dose samples.

Fig. 12 shows the TiNi sample surface after double implantation by N^+ and Ni^+ ions. The surface is rather rough (a = 0.8 – 1.2 мм) due to sputtering mainly by nitrogen atoms. This surface was subjected to electron- probe microanalysis. The following elements were detected in the near-surface layer (fig. 10): N (~2.1 at.%),O (~5.61 at.%, C (~0.58 at.%), Ni (~49.43 at.%), and Ti (~41 at.%). To detect Ti, we used another detector.

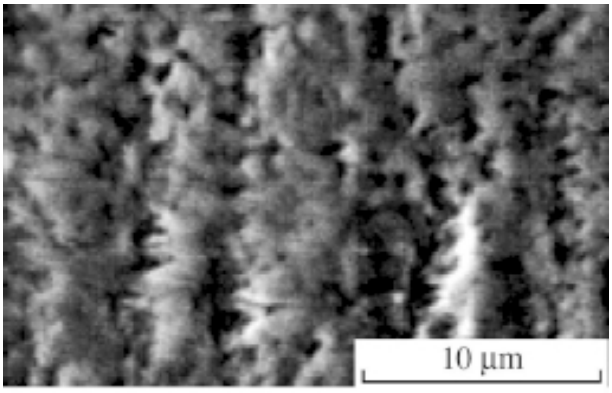

Fig. 12. TiNi sample surface implanted by nitrogen and nickel.

The low (as compared to the RBS data) titanium con-centration is caused by the larger depth of SEM as compared to EDS (which is 2.2 мм); moreover, the nitrogen ion range is at most 300 nm at the energies (60 – 70 keV) used in our experiments. Upon implantation, the elastic modulus increases insignificantly; however, after heat treatment, it increases to 236 ± 39 or 289 ± 80 GPa (i.e., by a factor of 4 – 4.5 compared to the initial state).

The coating demonstratedthe increased corrosion resistance in acidic and alkaline media in comparison with that of the non-implanted surface.

CONCLUSIONS

The development of TiNi based SMA thin films and their microactuators has achieved considerable progress in recent years. This was largely driven by a fast expansion of, in particular, microelectromechanical system and biological communities, in which the demand for novel actuators and biological applications has been growing dramatically. As such, a timely review of the important issues pertaining to the preparation of high quality and high performance shape memory TiNi thin films and the technical applications of these films is necessary.

We showed that the sequential double implantation of N^+ and Ni^+ ions into nitinol (TiNi) leads to the formation of a complex depth profile of the nitrogen con-centration, which is caused by the rejection of nitrogen ions from the region of the maximum Ni^+ ion losses (i.e., the region of the maximum Ni^+ ion concentration) to the region of residual tensile stresses. As a result of the implantation of N^+, Ni^+, W^+, and Mo^+ ions, the hardness after implantation increases by 30% com-pared to the initial state and the hardness after subse-quent thermal annealing at 550 °C for 2 h increases by a factor of 2.2. The SME changes because of the formation of nitrogen and carbon (carbonitride) layers as a result of N^+ implantation and because of a change in the con-centrations of Ti and Ni atoms due to the sputtering of Ni atoms, which is accompanied by a change in the martensite transformation temperature.

The martensitic form of equiatomic NiTi was implanted with N ions with the fluence 10^{18} cm^{-2} and 50 keV energy. To characterize the transformation sequence and transformation temperatures, the DSC measurements were carried out on an non-implanted as well as an implanted material. Both the non-implanted and ion-implanted NiTi alloys transform in two steps ($B_2 \rightarrow R \rightarrow B_{19}$) in the cooling direction and one-step transition ($B_{19} \rightarrow B_2$) in the heating process. To verify identifications of martensitic transformations in the NiTi alloys during heating and cooling, the X-ray structural investigations were performed.

The TEM structural characterization reveals the existence of the well-defined double-layer structure with different microstructure as well as different phase and chemical composition in the near-surface region of the ion-implanted NiTi alloy. From the surface to a depth of 80 nm, the sample has an amorphized structure in the form of two sub-layers: the first is a Ti- and N-rich nanocrystalline and/or

amorphous-like and the second – Ni-rich crystalline. In the depth of 80 – 160 nm the material has a defected Ti-rich crystalline microstructure and deeper – an unaffected grain structure of the parent material.

Some important issues pertaining to the preparation of high performance shape memory TiNi films using sputtering methods and their applications were reviewed in this paper. Successful application of TiNi thin films requires consideration of the following issues: preparation and characterization, residual stress and adhesion, frequency improvement, fatigue and stability, patterning and modeling of behavior. TiNi film based micoractuators will find potential applications in medicine, aerospace, automotive, and consumer products. Miniature TiNi actuated devices based on sputtered TiNi films are ready for the huge commercial market, especially for medical microdevices and implantable applications.

REFERENCES

1. Yongqing Fu, Hejun Du, Weimin Huang, Sam Zhang Min Hu. TiNi-based thin films for MEMS applications: a review//Sensors and Actuators. – 2004. – Vol. A 112. – P. 395-408.
2. Brunette D.M., Tengvall P., Textor M., Thomsen P. Titanium in Medicine. – Springer-Verlag: Berlin Heidelberg, Germany, 2001. – 1019 p.
3. Palel U., Kellet M.J. The misplaced double Jureteric Stent: technique for repositioning using nitinol “gooseneck” snare//Clinical Radiology. – 1994. – Vol. 49 (5). – P. 333-336.
4. Perez-Martin A.M., Vredenberg A.M., L. de Witet al. Carbide and nitride/carbide layers in iron synthesized by ion implantation//Mater. Sci. and Eng. – 1993. – Vol. B19. – P. 281-284.
5. Chrobak D., Morawiec H.Thermodynamic analysis of the martensitic transformation of plastically deformed NiTi alloy//Scr. Mater. – 2001. – Vol. 44. – P. 725-730.
6. ShabalovskayaS.,AndreggJ.,Van HumbeeckJ. Critical overview of Nitinol their modifications for medical applications //ActaBiomater. – 2008. – Vol. 4(3). – P. 447-467.
7. Pogrebnjak A.D., Bratushka S.N., Uglov V.V., Rusakov V.S., Beresnev V.M., Anischik V.M., Malikov L.V., Levintant N., Zukovski P. Structure and properties of Ti alloys after double implantation//Vacuum. – 2009. – Vol. 83, № 6. – S. 241-244.
8. Czeppe T., Levintant-Zayonts N., Swiatek Z., Michalec M., Bonchyk O., Savitskij G. Inhomogeneous structure of near-surface layers in the ion-implanted NiTi alloy//Vacuum. – 2009. – Vol. 83. – S. 214-219.
9. Kadyrzhanov K., Komarov F., Pogrebnjak A., Rusakov V.S.,Turkebaev T.E. Ion Beams and Ion Plasma Modification of Materials. – M.: Moscow State University Publishers. Russia, 2005. – 640 p.
10. Pogrebnyak A.D., Shpak A.P., Azarenkov N.A., Beresnev V.M. Structures and properties of hard and superhardnanocomposite coatings//Physics-Uspekhi. – 2009. – Vol. 52, No. 1. – P. 29-54.
11. Lavrentiev V.I., Pogrebnjak A.D. High-dose ion implantation into metals//Surf. and Coat. Techol. – 1999. –Vol. 99, No. 1-2. – P. 24-32.
12. Pogrebnjak A.D, Bakharev O., Pogrebnjak N.A., Tsvintarnaya Yu.V., Shablja V.T., Sandrik R., Zecca A. Certain features of high-dose and intensive implantation of Al ions in iron//Phys. Lett. – 2000. – Vol. A 265. – P. 225-232.
13. Pogrebnjak A.D., Michalev A., Pogrenjak N.A., Tsvintarnaya Yu.V., Lavrentiev V., Iljashenko M., Valyaev A., Bratushka S., Zecca A., Sandrik R. Evolution of vacancy defects and dislocations in surface layers of iron as a result of pulsed electron beam treatment//Phys. Lett. – 1998. – Vol. A241. – P. 357-363.
14. Pogrebnjak A.D., Kobzev A.P., Gritsenko B.P., Sokolov S., Bazyl E., Sviridenko N., Valyaev A., Ivanov Yu. Effect of Fe and Zr ion implantation and high-current electron irradiation treatment on chemical and mechanical properties of Ti-V-Al alloys//J. Appl. Phys. – 2000. – Vol. 87, No. 5. – P. 2142-2148.
15. Pogrebnyak A.D., Bratushka S.N., Levintant N., Erdybaeva N.K., Plotnikov S.V., Gritsenko B.P. Effect of high doses of N^+, $N^+ + Ni^+$, and $Mo^+ + W^+$ions on the physicomechanical properties of TiNi//Technical Physics. – 2009. – Vol. 54, No. 5. – P. 667-673.
16. Pogrebnjak A.D., Bazyl E.A. Modification of wear and fatigue characteristics of Ti-V-Al alloy by Cu and Ni ion implantation and high-current electron beam treatment//Vacuum. – 2001. – Vol. 64, No. 1. – P. 1-7.
17. Ivasishin O.M., Pogrebnjak A.D., Bratushka S.N. Nanostructured layers and coating formed by ion-plasma fluxes in titanium alloys and steels. – К.: Akademperiodyka, 2011. – 286 p.
18. Shirokov D.M., Bohac V. New computer iterative fitting program DVBS for backscattering analysis//Nucl. Instr. and Meth. in Psys. Res. – 1994. – Vol. 84 (B). – P. 497-506.
19. Oliver W.C., Pharr G.M. An improved technique for determining hardness and elastic modulus

using load and displacement sensing indentation experiments//J. Matter. Res. – 1992. – Vol. 7, No. 6. – P. 1564-1583.
20. Wayman C. M. Shape memoryand related phenomena//Prog. Mater. Sci. – 1992. – Vol. 36. – P. 203-224.
21. Filip P., Mazanec K. Effects of work hardening and heat treatment on the phase transformation behavior of Ti-50.6 at.% Ni alloys//Mater. Sci. Eng .– 1991. – Vol. A 141. – P. L5-L8.
22. Filip P., Mazanec K. Influence of work hardening and heat treatment on the substructure and deformation behavior of TiNi shape memory alloys //Scripta Metallurgica et Materialia. – 1995. – Vol. 32. – P. 1375-1380.
23. Miyazaki S., Igo Y., Otsuka K. Effect of thermal cycling on the transformation temperatures of TiNi alloys//ActaMetall. – 1986. – Vol. 34. – P. 2045-2051.
24. Pogrebnjak A.D., Kobzev A.P., Gritsenko B.P., Sokolov S., Bazyl E., Sviridenko N., Valyaev A., Plotnikov S.V. Effect of Fe and Zr ion implantation and high-current electron beam treatment on chemical and mechanical properties of Ti-V-Al alloy//Jpn. J. Appl. Phys. – 1999. – Vol. 38. – P. L248-L251.